Revista Mexicana de Astronomía y Astrofísica, **42**, 131–144 (2006)

THE USE OF K_S BAND PHOTOMETRIC EXCESSES TO INVESTIGATE H_2 EMISSION IN PLANETARY NEBULAE

G. Ramos-Larios, J. P. Phillips, and S. N. Kemp

Instituto de Astronomía y Meteorología
Universidad de Guadalajara, México

Received 2005 September 5; accepted 2006 February 17

RESUMEN

Se ha determinado la distribución de emisión H_2 en 14 (NP's), usando imágenes y fotometría publicadas en el catálogo infrarrojo de 2MASS. Esta técnica es aplicable solo bajo ciertas condiciones y requiere fotometría precisa,así como un exacto registro espacial entre las imágenes de banda K_S y H. Es, además, sólo aplicable para algunas fuentes, y excluye flujos en los cuales, la estrella central y el exceso de polvo caliente son apreciables. Los resultados para NGC 3132, NGC 6720, IC 4406 y M 2−9 son muy similares a imágenes previas de banda angosta, y confirman que la emisión H_2 está confinada a una envoltura delgada muy fragmentada. Se obtienen resultados similares para M 1−7, M 1−8 y M 3−5. Los perfiles espaciales también confirman que la emisión se extiende fuera de las cáscaras ionizadas primarias. Cuando las cáscaras son mayores y las NP's son más evolucionadas, entonces las extensiones fraccionales $\Delta\theta/\theta$ parecen ser más pequeñas. También son similares a los anchos radiales predichos para los perfiles de abundancias de H_2, y a los valores ΔR/R determinados a través de modelación magnetohidrodinámica de choques. Finalmente, parece haber evidencia para una evolución en este parámetro, tal que $\Delta\theta/\theta$ varía con el incremento de la medida de la envoltura d(H) como $\Delta\theta/\theta \propto$ d(H)$^{-2.2}$.

ABSTRACT

We have determined the distribution of H_2 emission in 14 planetary nebulae (PNe), using imaging and photometry published by the 2MASS infrared survey. This technique is only applicable under certain stringent conditions, and requires precise broad band photometry, and accurate spatial registration between the K_S and H band images. It is, in addition, only applicable to certain sources, and excludes outflows in which central star and grain thermal excesses are appreciable. Our results for NGC 3132, NGC 6720, IC 4406 and M 2−9 are closely similar to those of previous narrow band imaging, and confirm that H_2 emission is confined to narrow, highly fragmented shells. Similar results are obtained for M 1−7, M 1−8, and M 3−5. Our spatial profiles also confirm that the emission extends outside of the primary ionised shells. Where envelopes are large, and the PNe are more evolved, then the fractional extensions $\Delta\theta/\theta$ appear to be at their smallest. They are also similar to the radial widths predicted for H_2 abundance profiles, and to the values ΔR/R determined through magnetohydrodynamic modelling of shocks. There appears, finally, to be evidence for an evolution in this parameter, such that $\Delta\theta/\theta$ varies with increasing envelope size d(H) as $\Delta\theta/\theta \propto$ d(H)$^{-2.2}$.

Key Words: **ISM: GENERAL — PLANETARY NEBULAE: GENERAL**

1. INTRODUCTION

Planetary nebulae are known to contain large amounts of molecular material, with total masses ranging between 10^{-3} and 1 $M_\odot$ (Huggins & Healy 1989). The largest H I/H II mass ratios are most commonly to be found where shell masses are large, as is the case with Peimbert Type I PNe and (the

related) bipolar outflows (e.g., Huggins et al. 1996; Phillips 2005). Similarly, such ratios are likely to depend upon the evolutionary status of the nebulae, and to be larger in sources which have low central star temperatures, and are more dense and less evolved.

The most effective tracers of this gas have been found to be molecules such as CO, CS, HCO^+ and HCN (e.g., Oloffson et al. 1982; Deguchi et al. 1990; Bachiller et al. 1989; Josselin & Bachiller 2003) all of which have rotational transitions at millimetric and submillimetric wavelengths. Analysis of their abundances has permitted an insight into the chemical evolution of the shells (e.g., Bachiller et al. 1997). By contrast, molecular hydrogen, which is the most abundant molecular species, has proven exceptionally difficult to observe. The absence of permanent magnetic or electric dipole moments results in an absence of rotational transitions at longer wavelengths, and one of the few ways in which they may be detected is through rotational-vibrational transitions in the NIR.

The $\nu = 1{-}0$ S(2) ($\lambda = 2.034$ μm), $\nu = 1{-}0$ S(0) (2.223 μm), $\nu = 2{-}1$ S(1) (2.248 μm) and (above all) the $\nu = 1{-}0$ S(1) (2.122 μm) transitions appear to be particularly strong (e.g., Davis et al. 2003; Zuckerman & Gatley 1988; Storey 1984; Vicini et al. 1999; Shupe et al. 1998), and have been detected in more than 60 outflows to date (see e.g., Kastner et al. (1996) for a summary of detections prior to 1996). Spatial mapping shows that much of this emission is associated with the outer limits of the ionised shells, close to the H I/H II interface (e.g., Graham et al. 1993), and has a similar distribution to that of [O I] (Balick et al. 1990) and [N II] (Bohigas 2001; Guerrero et al. 2000; Schild 1995). The most likely explanations for these transitions involve UV pumping within photodissociative zones (e.g., Natta & Hollenbach 1998; Black & Dalgarno 1976; Black & van Dishoeck 1987; Burton, Hollenbach, & Tielens 1990; Sternberg & Dalgarno 1989) and/or local shock activity (see e.g., Hollenbach & McKee 1989; Draine et al. 1983). There appears little doubt that the former process is important in many, if not most PNe (e.g., Hora, Latter, & Deutsch 1999; Hora & Latter 1994; Vicini et al. 1999; Shupe et al. 1998), although Davis et al. (2003) note that shocks are dominant in NGC 7048, and have a partial role in sources such as NGC 6886, Hb 5, and NGC 6445. Similarly, the kinematics of certain younger sources (such as CRL 2688) testify to appreciable levels of shock excitation (Kastner et al. 2001; Sahai et al. 1998).

Almost all of the maps published so far have been acquired through use of narrow band filters, and this is certainly the most sensitive (and useful) technique for undertaking this type of analysis. We would like to point out that H and K_S broad band imaging may also be used for this purpose, however. Although such procedures are not as wavelength discriminatory, and have lower levels of sensitivity, they permit us to map H_2 in sources for which levels of emission are high. A comparison of our present mapping with prior (narrow band) results will be shown to indicate high levels of correspondence, and confirm the viability of the procedure.

We shall confirm that H_2 emission is located close to (and just outside of) the primary ionised shells, and has a fractional extension $\Delta\theta/\theta$ which appears to depend upon the sizes of the envelopes. We shall also confirm the presence of narrow, highly knotted structures within NGC 3132, NGC 6720, and IC 4406, reveal the presence of similar morphologies within M 1−7, M 1−8, and M 3−5, and present profiles and maps for a further seven PNe.

2. DETERMINING THE DISTRIBUTION AND INTENSITIES OF K_S BAND EXCESSES

Ramos-Larios & Phillips (2005) have demonstrated that most larger, spatially resolved PNe tend to congregate within a very restricted regime of the NIR colour plane. The fluxes in these sources appear to be dominated by thermal Bremsstrahlung and H I Brackett line emission, and imply mean indices $<(J - H)_0> \cong -0.013\pm0.013$ mag, and $<(H - K_S)_0> \cong 0.642\pm0.011$ mag. Similarly, the dispersions in the indices are found to be of order $\sigma((J - H)_0) \cong 0.093$ mag and $\sigma((H - K_S)_0) \cong 0.079$ mag, although most if not all of this scatter is attributable to photometric errors, and to uncertainties in the extinction coefficient c. It therefore follows that the intrinsic indices of these sources are likely to be very closely comparable. Differences in $(H - K_S)_0$ are probably no greater than $\cong 0.03$ mag, depending upon the level of nebular excitation.

Such a result is consistent with what would be expected. The H band (between 1.51 and 1.80 μm) is dominated by both thermal continuum radiation, and the B10 through B21 Brackett lines of H I. It is only very weakly affected by other transitions. The $3^3P{-}4^3D$ line of He I ($\lambda = 1.7002$ μm) is particularly strong in lower excitation nebulae, whilst the 7−12 transition of He II ($\lambda = 1.692$ μm) is found in higher excitation sources such as NGC 7027 (see e.g., Treffers et al. 1976; Zhang & Kwok 1992). Neither of these lines makes an appreciable contribution

to overall flux levels, however. For instance, if one takes the nebula IC 418 as fairly typical of lower excitation outflows, then we find that the He II and He I transitions contribute $\sim 0.4\%$ to the H band fluxes (a similar value is obtained for IC 5117, also observed by Zhang & Kwok). By contrast, and at the other extreme, these lines contribute $\sim 0.9\%$ to fluxes in NGC 7027. From one end of the excitation range to the other, therefore, it is clear that H I line+continuum emission dominates H band fluxes.

The K_S band is located between 2.00 and 2.32 μm. Apart from the He II 7−10 transition at 2.189 μm, and the 2^1S-2^1P and $4s^3S-3p^3P^0$ transitions of He I at 2.059 and 2.113 μm, the flux is dominated by Bremsstrahlung continuum emission, and the λ2.166 μm Brγ line of H I (e.g., Treffers et al. 1976; Zhang & Kwok 1992; Rudy et al. 2001). It is clear, yet again, that the secondary (He I + He II) transitions are expected to be weak. They contribute $\sim 3.5\%$ to K_S band fluxes in NGC 7027, and $\sim 1/3$ of this in the sources investigated by Davis et al. (2003). Even more important from the point of view of the present analysis, however, is that the brightest of these lines, the 2.058 μm transition of He I, is some ≈ 20 to 40 times weaker than the excesses we shall be considering below. Neither this, nor the other transitions, can be responsible for the trends discussed in § 4.

Although CO transitions at $\lambda \geq 2.294$ μm may cause some contamination at the limits of the K_S band, such emission tends to occur in protoplanetary sources having late spectral types (mid-G or later; see e.g., Kwok 2000). The impact of such transitions is therefore likely to be small to negligible. Our present sources tend to be evolved and/or have high Zanstra temperatures T_Z (e.g., Phillips & Ramos-Larios 2005; Phillips 2003), for instance. Similarly, the transitions occur in a portion of the spectrum where atmospheric and filter transmissions are low.

Finally, it is worth making two further points concerning the transitions within these bands. The Brackett line strengths depend upon nebular densities, temperatures, and He/H abundance ratios. Since the latter two parameters are similar in most PNe, and both lines and continua have similar dependencies upon density, then Brackett to continuum emission ratios should be reasonably invariant. Similarly, we note that that none of these transitions (H I, He I or He II) would be expected to extend outside of the ionised shell − a trend which is again at variance with the excesses described in § 4.

Two conclusions therefore follow from the discussion above. Firstly, the He I, He II, and CO lines are likely to be weak compared to K_S and H band fluxes. Similarly, they are also very much weaker than the K_S excesses to be considered below, as well as possessing differing spatial distributions.

Given this situation, then it follows that where there is excess emission $\Im(K_S)$ in the K_S band, and no corresponding excess at H, then to a good approximation

$$\log\left[\frac{\Im(K_S)}{Wm^{-2}Hz^{-1}}\right] = -9.367 - 0.4H_{OBS} + \log(\Delta K_S) + 0.150c + 0.4 < (H-K_S)_{00} > + \log[\exp(2.303\{0.4\ (H-K_S)_{OBS} - 0.4 < (H-K_S)_{00} > -0.058c\}) - 1] \quad (1)$$

where terms subscripted OBS correspond to the observed magnitudes, $\Delta\ K_S = 0.32$ μm is the width of the K_S filter bandpass, and $< (H-K_S)_{00} > \cong 0.642$ mag is the zero point colour index cited above. The extinction correction factors are calculated using the ratios $A_H/A_V = 0.176$ and $A_K/A_V = 0.108$ taken from Cardelli, Clayton, & Mathis (1989), and assume that $E_{B-V}/c = 1.46$ and $A_V/E_{B-V} = 3.1$ (Pottasch 1984).

Systematic errors in the use of this equation depend upon uncertainties in $< (H-K_S)_{00} >$ and c, but are likely to be relatively modest. Where observed values $(H-K_S)_{OBS}$ are greater than 1, for instance, which is characteristic of the H_2 emission regimes observed here, then for $\sigma(c) \sim 0.1$ and $\sigma(< (H-K_S)_{00} >) \sim 0.03$ mag we find that biases in $\Im(K_S)$ are unlikely to exceed $\sim 5\%$. Where $(H-K_S)_{OBS}$ dips down to ~ 0.9, then maximum biases increase to $\sim 10 \rightarrow 15\%$.

Such a situation, where excesses are appreciable and occur in the K_S band alone, would arise where the H_2 $\nu = 1-0$ S(1), $\nu = 2-1$ S(1) and other transitions are strong (see § 1); indeed, we are unaware of any other mechanism which would be capable of replicating such a trend. The only exception may occur where there exist hot dust continua (see later this section), although this would lead to quite different $(J-H)/(H-K_S)$ colours to those observed here (Phillips & Ramos-Larios 2005).

It follows that accurate H and K_S mapping should enable us to trace the distribution of H_2 emission, providing that the relevant transitions are sufficiently intense. The requirements necessary for such mapping will be described later this section. Suffice to say that such constraints are satisfied by the 2MASS infrared survey (see § 3). Although the sensitivity of this survey is somewhat restricted, and limits our analysis to higher surface brightness sources

alone, it is nevertheless sufficient to permit mapping of a reasonably large number of sources.

It is also possible to undertake such an analysis using J and K_S photometric results as well. Such a procedure would be open to much larger uncertainties, however. Corrections for IS extinction are ~ 2.6 times as large, so that errors in c have a significantly larger overall effect. More important, however, is the effect of the $2p^3P^0-2s^3S$ transition of He I at $\lambda = 1.083$ μm. This is located at the limits of the 2MASS filter passband, and affected by low (and variable) levels of atmospheric transmission (Carpenter 2001). Both of these factors tend to reduce the influence of this transition. Nevertheless, there is clear evidence that it may enhance fluxes within the J photometric band, and lead to reduced indices $(J-H)_0$ (Peña & Torres-Peimbert 1987; Whitelock 1985; Ramos-Larios & Phillips 2005). Such a line would also have the effect of compromising our analysis of H_2 emission.

It is clear that such H_2 mapping is only possible where the independent H and K_S results have closely similar resolutions, are spatially well registered (i.e., there is little displacement between the maps), and where values of S/N are large. In addition to this, it is also necessary to place various constraints upon the outflow sources to be mapped.

Such an analysis would be inappropriate, for instance, where there is strong (and strongly variable) local extinction, such as appears to be the case in NGC 7027, BD+30°3639, NGC 6302 and other nebulae (e.g.. Atherton et al. 1979; Lame et al. 1995; Matsuura et al. 2005). Unless the variation in c is very well known, and factored into Eq. (1), then the use of a uniform average may lead to appreciable errors. It is also important that the H and K_S band maps are not too strongly affected by background sources, such as may occur where nebulae are located close to the Galactic plane.

Where central star emission is appreciable, then this may result in excesses within the H and K_S photometric bands. Unless care is taken to correct for this, then this would also vitiate any such analysis. Such a situation is likely to be particularly critical in the case of compact PNe. Where sources are larger, however, then this problem is usually very much alleviated. The central stars of NGC 3132 and NGC 6720 appear bright at NIR wavelengths, for instance, although this has little impact upon mapping of the more extended H_2 emission (see later).

It is clear that warm dust emission is often spatially extended, and may even be detected outside of the primary ionised shells (see e.g., Phillips & Ramos-Larios 2005). This emission is usually identified through changes to both the $(J-H)_0$ and $(H-K_S)_0$ indices. Although such continua have been detected in only a few PNe (i.e., in SwSt 1 (de Marco et al. 2001); Mz 3 (Smith 2003); A 30 (Borkowski et al. 1994); NGC 2346 (Costero et al. 1986; Su et al. 2004); Cn 1−1 (Bhatt & Mallick 1986); IC 5117 (Rudy et al. 2001); and in IC 418, BD+30°3639, NGC 40 and various other sources (Willner, Becklin, & Visvanathan 1972; Willner et al. 1979; Cohen & Barlow 1974; Phillips et al. 1984; Phillips & Ramos-Larios 2005), these nebulae should also be excluded from any such analysis.

We have finally required that the sources in our analysis should have been previously detected in H_2 S(1), and/or correspond to the H_2 candidates identified by Phillips & Ramos-Larios (2005). This is not a prerequisite for all such analyses, but enables us to establish the veracity of the trends to be described in § 4. In particular, it ensures that levels of H_2 emission are reasonably large, and very much greater than those of other "contaminating" transitions.

These constraints, together with the limited sensitivities of the survey, restrict the numbers of nebulae which may be analysed. We have nevertheless been able to produce profiles and mapping for a total of 14 PNe, including five sources for which such maps already exist. This overlap is useful, since it permits us to check the accuracy of our results.

In particular, we note that our maps of NGC 6720, NGC 3132, and IC 4406 are very closely similar to prior narrow band imaging by Storey (1984), Greenhouse, Hayward, & Thronson (1988), Kastner et al. (1994), Latter et al. (1995), and Allen et al. (1997). All of them reveal similar levels of intensity and morphology, and confirm the tendency for H_2 emission to be concentrated towards the limits of the outflows. Where there are differences, then they may be attributed to variations in the limiting sensitivities, in the levels of the contours, and from the fact that our current mapping includes various H_2 transitions (see § 1).

Details of the data base used for this mapping are provided in § 3, whilst a further discussion of the results is to be found in § 4.

3. THE 2MASS DATA BASE

We have employed 2MASS H and K_S band imaging in order to evaluate the distribution of H_2 emission in 14 outflow sources: Hb 12, J 900, M 1−7, M 1−8, M 1−13, M 1−20, M 2−9, M 2−43, M 2−49, M 3−5, Me 2−2, NGC 3132, IC 4406,

TABLE 1

PARAMETERS FOR H_2 EXTENSION OUTSIDE OF THE IONISED SHELLS

Source	G.C.	D kpc	$\theta(H)$ arcsec	θ(RAD) arcsec	d(H) pc	$\Delta\theta/\theta$
M 1−20	006.1+08.3	5.90	0.98	1.9	0.028	2.68±0.20
M 2−9 (S)	010.8+18.0	1.82	8.06	···	0.071	0.35±0.04
M 2−9 (N)	010.8+18.0	1.82	10.69	···	0.094	0.21±0.04
M 2−43 (E−W)	027.6+04.2	5.00	1.33	1.3	0.032	1.70±0.19
NGC 6720 (N−S)	063.1+13.9	0.60	60.7	70	0.177	0.046±0.017
NGC 6720 (E−W)	063.1+13.9	0.60	78.7	70	0.230	0.028±0.015
M 2−49 (N−S)	095.1−02.0	6.47	1.42	2.5	0.045	1.14±0.18
Me 2−2 (N−S)	100.0−09.7	8.56	1.42	1.4	0.059	0.53±0.18
Hb 12 (N−S)	111.8−02.8	10.46	0.54	0.5	0.025	3.29±0.35
Hb 12 (E−W)	111.8−02.8	10.46	0.4	0.5	0.020	6.94±0.43
M 1−7 (E−W)	189.8+07.7	4.50	8.83	11	0.193	0.37±0.05
M 1−13 (E−W)	232.3−01.8	4.51	8.38	10	0.183	0.59±0.06
NGC 3132 (N−S)	272.1+12.3	0.64	49.3	45	0.153	0.033±0.021
NGC 3132 (E−W)	272.1+12.3	0.64	44.4	45	0.138	0.088±0.021
IC 4406 (N−S)	319.6+15.7	1.50	27.1	34.5	0.198	0.086±0.028

and NGC 6720. The survey was undertaken between June 1997 and February 2001, using 1.3 m telescopes located at Mt. Hopkins Arizona, and the CTIO in Chile. Each telescope was equipped with a three-channel camera, each channel consisting of a 256×256 array of HgCdTe detectors. This permitted simultaneous observations of the sky in the J(1.25 μm), H(1.65 μm), and K_S(2.17 μm) bands.

Pixel sizes are 1 arcsec, whilst measurements of field star images shows them to be circularly symmetric, and to have a typical FWHM of 3.3 arcsec. This latter parameter varies by $\pm 0.3 \rightarrow 0.4$ arcsec depending upon seeing at the time of observation. Similarly, 3σ surface brightnesses limits also vary somewhat, but are of general order 20.2 mag arcsec^{-2} at H, and 19.5 mag arcsec^{-2} at K_S.

It is important, in subtracting one image from another, that the images are spatially well registered. Quoted positional accuracies are of order 70−80 mas (see the 2MASS web page at http://pegasus.phast.umass.edu), although we have noted occasional mis-registrations of up to 0.3 arcsec. This is extremely small ($\sim 10\%$ of the resolution limit), however, and unlikely to compromise the accuracy of the mapping described in § 4.

Finally, sources were selected according to the criteria outlined in § 2. Our profiles for these nebulae are illustrated in Figures 1 to 3, and pass through the geometric centres of the shells (the central star where visible). The one exception to this is M 2−9, where the images were found to be much affected by diffraction spikes. The profiles, for this case, pass transversely across the northerly and southerly lobes (Fig. 2), a procedure which restricts distortion of our results to the central scan pixels alone.

Two superimposed profiles are shown in each of the panels. One, representing the H band profile, is denoted by the dashed curves. This is indicative of the distribution of H ionised emission (see § 2). The other (solid) curves correspond to H_2 emission, estimated according to the procedures in § 2. Both sets of curves are normalized to their peak intensity levels.

Each data point has also been averaged over several pixels orthogonal to the direction of the profile, the degree of averaging depending upon the sizes of the sources. Thus, each value in the N−S profile for IC 4406 is a median of 10 pixels along the E−W axis. Further details of the averaging may be found in the caption to Fig. 1.

Maps for selected outflows are illustrated in Figures 4 to 6, and correspond to nebulae in which the distribution of H_2 emission is spatially well resolved, and S/N ratios are high. The lower contours are for the most part set at the 2σ noise level. Those in the H map of NGC 6720 are somewhat higher, however,

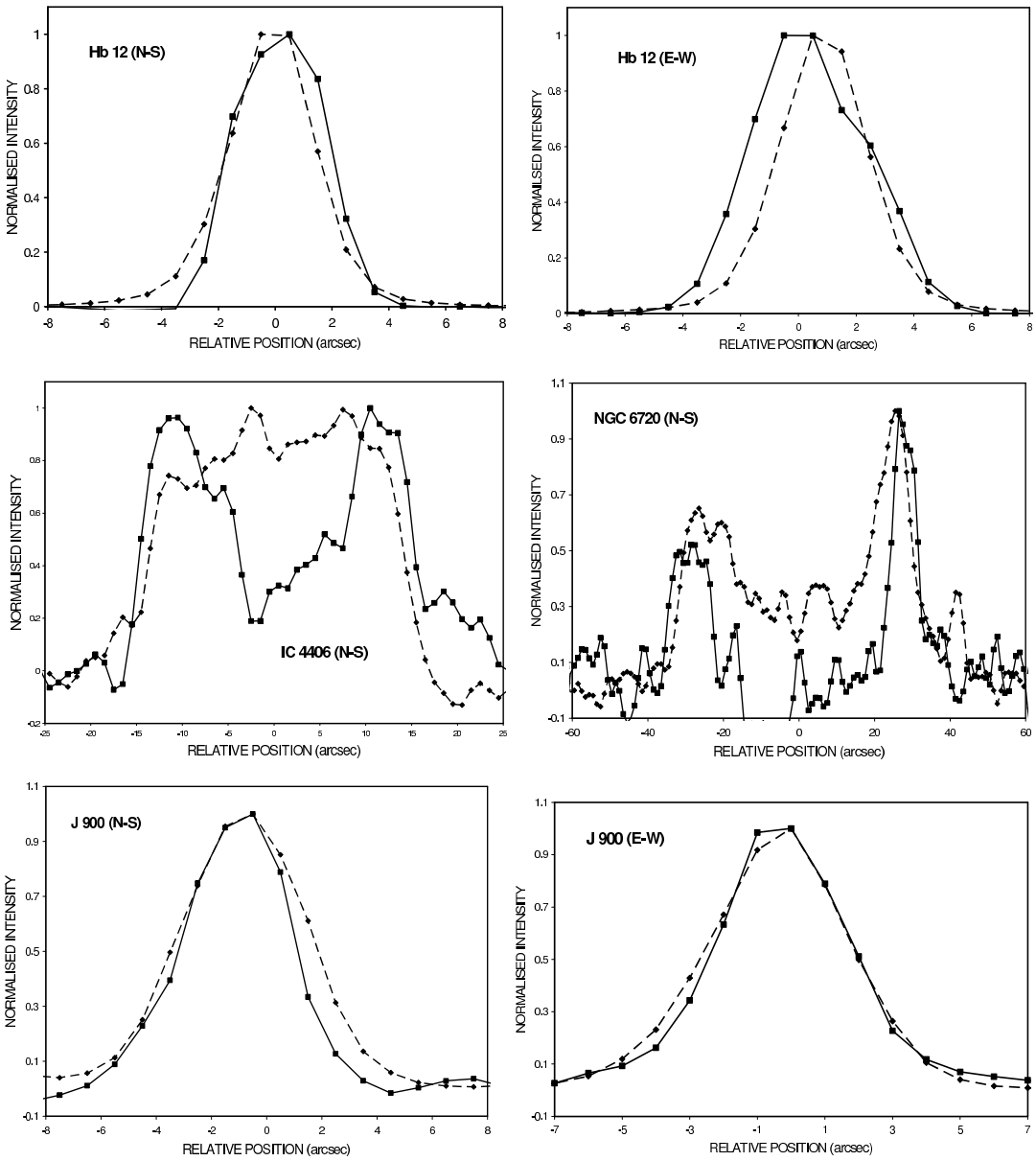

Fig. 1. Spatial profiles of H_2 (solid curves) and H photometric emission though various PNe shells, normalized to their peak intensities. The individual data points represent means of several pixels along the orthogonal axes (see text). The pixel averaging is as follows: Hb 12 (2 pixels); IC 4406 (10 pixels); NGC 6720 (9 pixels); and J 900 (4 pixels). Most scans are taken through the centres of the nebulae. The one exception to this is M 2−9 (see Fig. 2), where the profiles represent emission located between 12 and 20 arcsec north of the central star (M 2−9(E−W)N), and between 6 and 14 arcsec south of the central star (M 2−9(E−W)S).

and designed to illustrate the difference in widths between the H_2 and gas thermal emission shells. The individual results are further discussed in § 4.

4. MAPPING RESULTS AND PROFILES

We have illustrated H_2 profiles and maps for 13 PNe in Figs. 1 to 6, together with the variation of fluxes within the H photometric band. These latter results are representative of trends in H ionised emission, as explained in § 2.

Several results are immediately apparent. It is clear, in the first place, that the distributions of H_2 and H ionised emissions are often quite distinct, as has been noted several times previously in other such

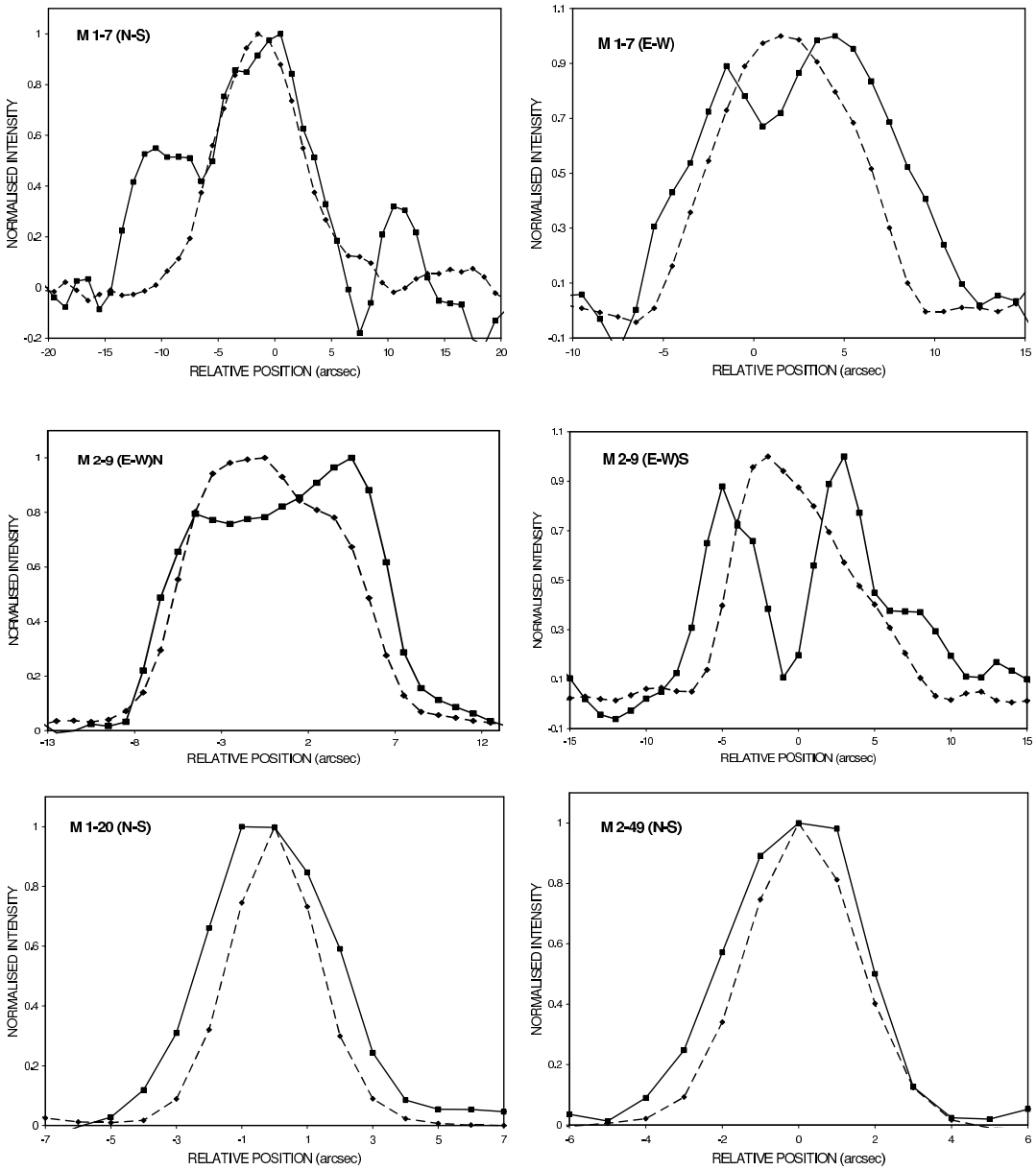

Fig. 2. As in Fig. 1, but for the sources M 1−7, M 2−9, M 1−20, and M 2−49. The pixel averages are as follows: M 1−7 (5 pixels); M 2−9 (9 pixels); M 1−20 (3 pixels); and M 2−49 (2 pixels).

analyses (see e.g., Guerrero et al. 2000; Graham et al. 1993; Beckwith, Persson, & Gatley 1978; Hora & Latter 1994). The H_2 emission often extends over a broader spatial range, and is to be found outside of the primary ionised shells. This is the case for Hb 12, M 1−7, M 1−20, M 2−43, and Me 2−2. It is also confirmed for other sources (IC 4406, M 2−9, NGC 6720, and NGC 3132) in which such trends have previously been detected.

The only case which appears to violate this trend is J 900. However, we note that this source also has a weaker external H_2 envelope, with dimensions very much greater than those of the principal ionised regime (Dinerstein et al. 1989; Shupe et al. 1995).

The results of a more detailed analysis of source extensions is provided in Table 1, where we show the fractional H_2 widths $\Delta\theta/\theta = (\theta(H_2) - \theta(H))/\theta(H)$ after deconvolution of our results. θ (H_2) is the FWHM of the H_2 emission profile, and θ(H) is the corresponding dimension in the H band. Errors are based upon an analysis of uncertainties in profile widths, and the way that these propagate into

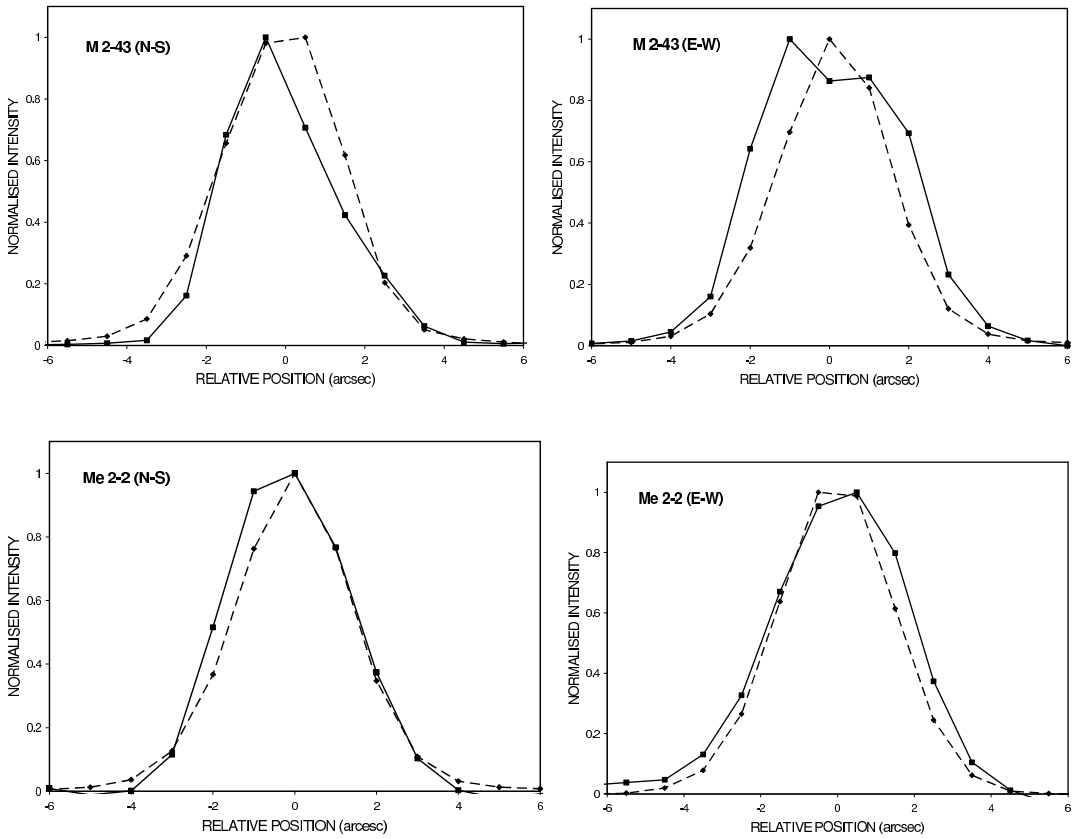

Fig. 3. As in Fig. 1, but for the sources M 2−43 and M 2−2. The pixel averages are as follows: M 2−43 (5 pixels); and Me 2−2 (2 pixels).

the ratio $\Delta\theta/\theta$. It is clear that fractional errors $\sigma(\Delta\theta/\theta)/(\Delta\theta/\theta)$ increase with decreasing $\Delta\theta/\theta$.

We have selected sources in which the H II region is closely enveloped by the H_2 emission zone – the majority, as it turns out, of the sources considered here. We have also quoted independent radio dimensions θ(RAD) derived from radio interferometry. These are mostly culled from the compilation of Zhang (1995), as well as from observations by Johnson, Balick, & Thompson (1979) and Miranda, Torrelles, & Eiroa (1995). Note that we have not included comparative dimensions for M 2−9, since our values θ(H) correspond to lateral slices across the lobes.

The deconvolved widths θ(H) are mostly similar to the values θ(RAD) in Column 5. Some differences occur because the comparative values refer to mean dimensions, and/or to differing intensity levels. It is also possible that disparities arise in smaller sources because of errors in spatial deconvolution.

Interferometric results also tend to filter out larger spatial frequencies; frequencies which are preferentially detected in the current mapping. This may lead to estimates θ(RAD) which are less than θ(H).

Taken as a whole, however, we find that $<\theta(\mathrm{H})>/<\theta(\mathrm{RAD})> \cong 0.97\pm0.33$ for larger sources (θ(H) $>$ 8 arcsec), and $<\theta(\mathrm{H})>/<\theta(\mathrm{RAD}> \cong 0.75\pm0.23$ where θ(H) $<$ 1.5 arcsec; an agreement which is better than might have been expected given the spatial resolution of the survey.

Finally, the distances to these sources are taken from a mix of directly observed values (i.e., those based upon trigonometric parallax, spectroscopic parallax and the like; see Phillips 2002a), and the statistical estimates of Phillips (2004) and Zhang (1995). These estimates, together with the angular sizes θ(H), are used to determine the dimensions d(H) of the nebular shells (Column 6).

It is immediately apparent that values $\Delta\theta/\theta$ tend to be smaller where source angular and physical dimensions are large, and range between ~ 0.028 and 0.2. These estimates are similar to the modelling results of Aleman & Gruenwald (2004), in which the variation of $n(H_2)/n(H)$ is determined

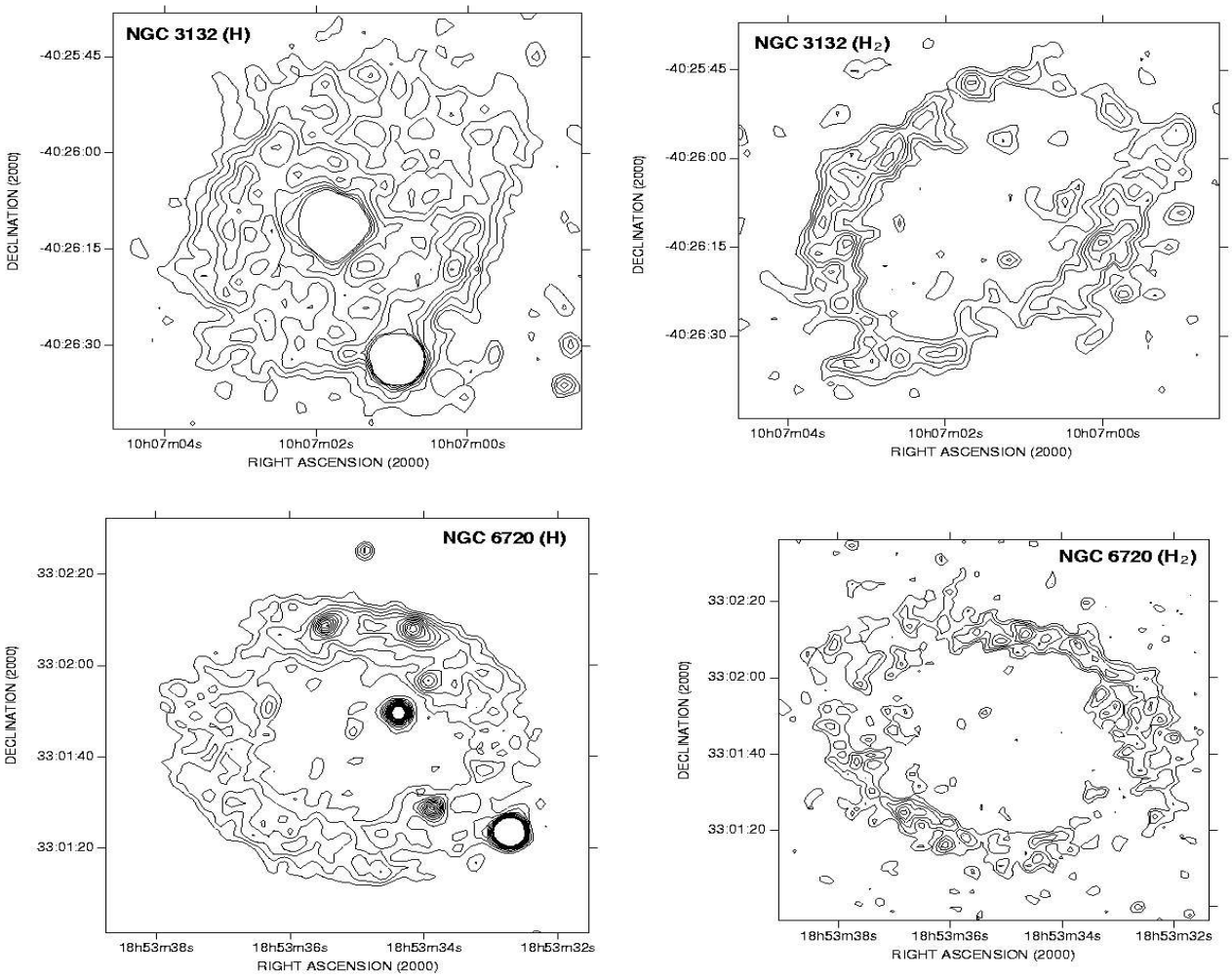

Fig. 4. H_2 and H band emission maps for various PNe. The contours are in all cases linear, with the lowest values set at the 2σ sky noise level. The only exception to this is the H band imaging of NGC 6720, for which the lowest contour is set at 4.8σ . This permits us to emphasise differences between the H II and H_2 shells. The surface brightnesses of the lowest contours, and the contour intervals, are respectively as follows: NGC 3132 (H) (4.84 10^{-15}; 2.88 10^{-15}); NGC 3132 (H_2) (4.76 10^{-15}; 2.24 10^{-15}); NGC 6720 (H) (8.07 10^{-15}; 2.59 10^{-15}); and NGC 6720 (H_2) (3.73 10^{-15}; 1.81 10^{-15}). All surface brightnesses are in units of ergs cm^{-2} arcsec^{-2}.

as a function of nebular radius. The latter authors find that n(H_2) is sharply peaked within the inner photo-dissociative regime, and occupies a radial range $\Delta R/R_S \approx 0.15$ (where R_S is the radius of the ionised shell). Densities fall-off precipitously outside of this regime. Much here depends upon how the molecules are excited, however, and how the variation in n(H_2) is related to the projected distribution of emission. The correspondence between model and observations is encouraging, if not yet confirmed.

The case of magnetohydrodynamic shock waves has been treated by Draine et al. (1983), among others. It is evident that the precise structures of the shock fronts, their cooling properties and emission characteristics depend upon a broad range of ill-defined parameters − or at least, ill-defined for the case of PNe H I envelopes. However, for neutral clouds with densities similar to those of PNe (n(H) $\sim 10^3 - 10^4$ cm^{-3}), and for shock velocities of order $\sim$ 25 km s^{-1}, it would seem that shock heating is important over depths approaching 10^{17} cm. Where sources are large, then this would imply ratios $\Delta\theta/\theta \sim 0.1 \rightarrow 0.2$ comparable to those observed here.

Errors in $\Delta\theta/\theta$ increase as source sizes decrease. Nevertheless, there is little doubt that our overall

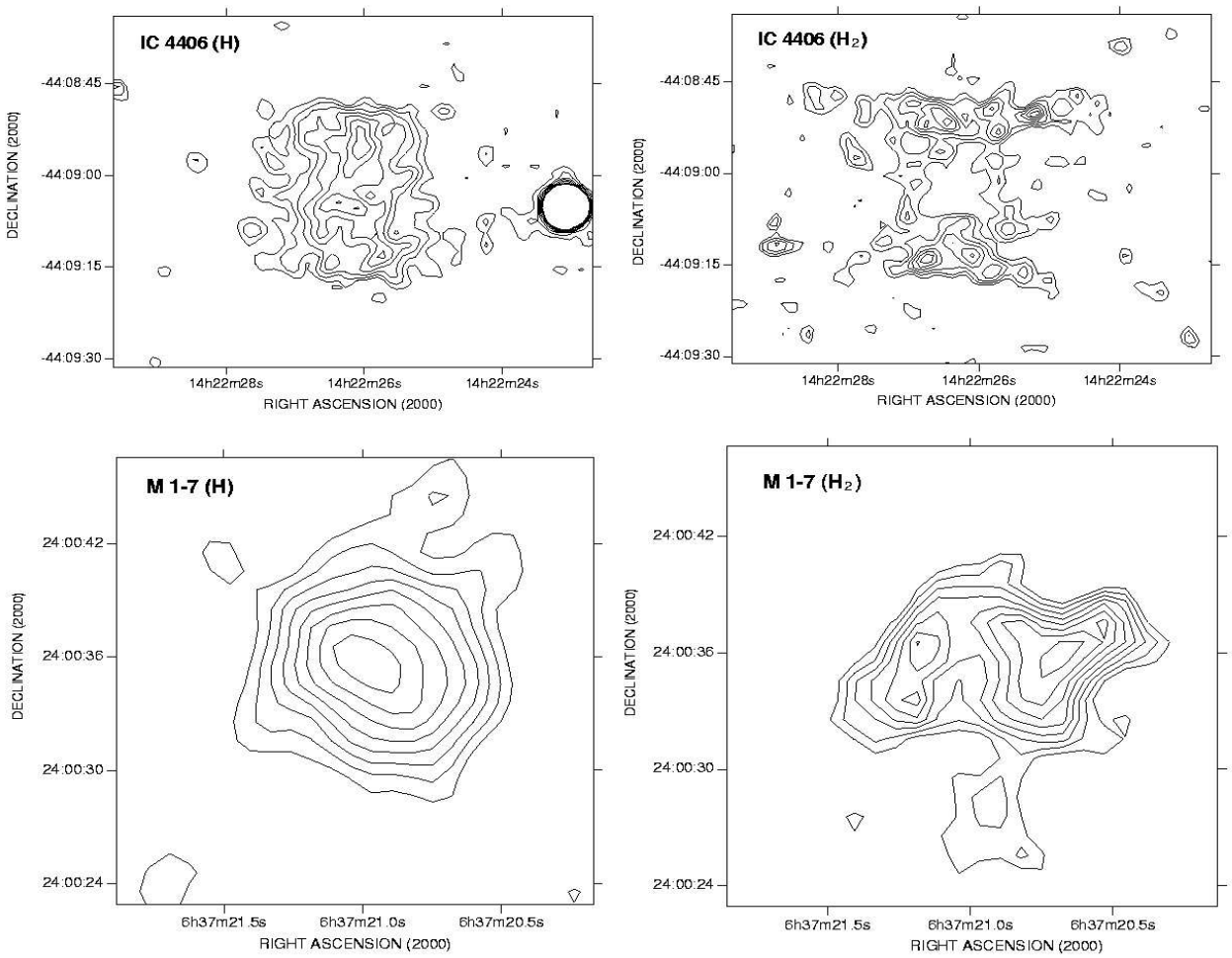

Fig. 5. As in Fig. 4, but for the sources IC 4406 and M 1−7. The contour parameters are as follows: IC 4406(H) (4.83 10^{-15}; 2.36 10^{-15}); IC 4406(H_2) (4.39 10^{-15}; 1.68 10^{-15}); M 1−7 (H) (3.31 10^{-15}; 2.44 10^{-15}); M 1−7 (H_2) (3.37 10^{-15}; 7.08 10^{-16}); in units of ergs cm^{-2} arcsec^{-2}.

trends are accurate. We find that $\Delta\theta/\theta$ increases markedly as θ(H) decreases; indeed, the differences between the H_2 and H II shells would be all but indistinguishable were this not the case. We have also illustrated this trend in Figure 9, where $\Delta\theta/\theta$ is represented against the linear dimensions of the nebulae d(H). It is clear that there is a well defined gradient such that $\Delta\theta/\theta \propto \mathrm{d(H)}^{-2.23}$. The degree of correlation is remarkable given the uncertainties in distance.

There is therefore some prima-facie evidence for an evolution in $\Delta\theta/\theta$, related, perhaps, to the relative importance of the differing excitation mechanisms. It may be that whilst UV excitation is more important in young sources, and extends throughout the exterior neutral envelopes, it is shocks which become more dominant as nebulae become larger. Such trends would be unlikely to arise as a consequence of shock excitation alone, however. For this case, the size of the excitation zone depends upon densities n(H). Since these are likely to be larger in more compact PNe, one would then expect that $\Delta\theta/\theta$ would be smaller where source dimensions were less: that gradients dlog($\Delta\theta/\theta$)/d(log(d(H)) would be > 0. Such a result would clearly be in conflict with the trends presented here.

Shock velocities may also vary with nebular radii, and this would undoubtedly affect the widths of the H_2 emission zones. The nature of such variations is at present unknown, although we note that expansion velocities in evolved nebulae (i.e., those having radii > 0.02 pc) do not seem to vary greatly (Phillips 2002b). Modelling of velocities V_I at the H I/H II interface, on the other hand, appears to indicate that V_I may be smaller in less evolved sources (e.g., Marigo et al. 2001).

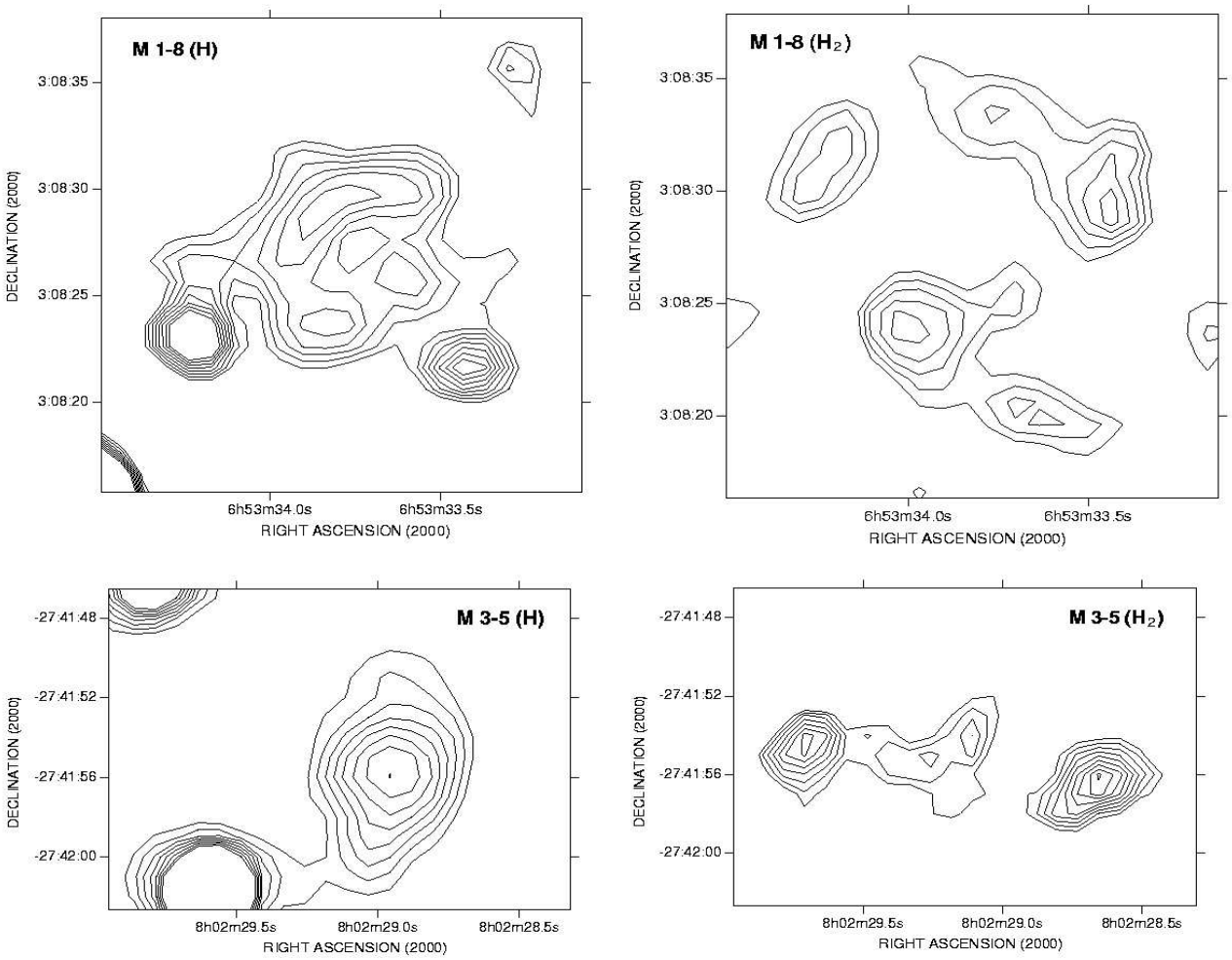

Fig. 6. As in Fig. 4, but for the sources: M 1−8 and M 3−5. The contour parameters are as follows: M 1−8 (H) (5.05 10^{-15}; 1.08 10^{-15}); M 1−8 (H_2) (4.56 10^{-15}; 1.35 10^{-15}); M 3−5 (H) (4.65 10^{-15}; 2.86 10^{-15}); M 3−5 (H_2) (5.01 10^{-15}; 7.75 10^{-16}); in units of ergs cm^{-2} arcsec^{-2}.

The mapping results also reveal various other distinctive morphological characteristics. Maps of NGC 3132, NGC 6720, and IC 4406 have been published by Storey (1984), Greenhouse et al. (1988), Kastner et al. (1994), Latter et al. (1995), and Allen et al. (1997). The present results amply support these results, and confirm the narrowness of the primary H_2 emission regimes, and the high levels of shell fragmentation. It is clear that condensations are occurring over scales less than the current resolution limit of $\sim$ 3 arcsec.

Apart from these cases, it is also interesting to take note of the relative H band and H_2 distributions for M 1−7, M 1−8, and M 3−5. Although all of these sources are compact, it is nevertheless clear that the H_2 envelopes extend outside of (and envelope) the primary ionised shells. This is perhaps more clearly seen in Figs. 7 and 8, where we have superimposed the two sets of results. It would also appear that the H_2 shells are again highly fragmented.

M 3−5 is particularly interesting in this regard, since apart from the emission being located on either side of the ionised zone, there also appears to be a strong knot located towards the east, and separated from the nebula by 9.8 arcsec. Further investigation of this "ansa" would be of considerable interest. The saturated south-eastern H band structure is a nearby field star, and has no connection with the source.

The only previous H_2 imaging of the source was by Bohigas (2003), and this seems to imply a somewhat different overall structure; the H_2 forms an annular ring at the centre of the nebula, with dimensions significantly less than that of the [N II] λ6584 envelope. There is some uncertainty, however, as

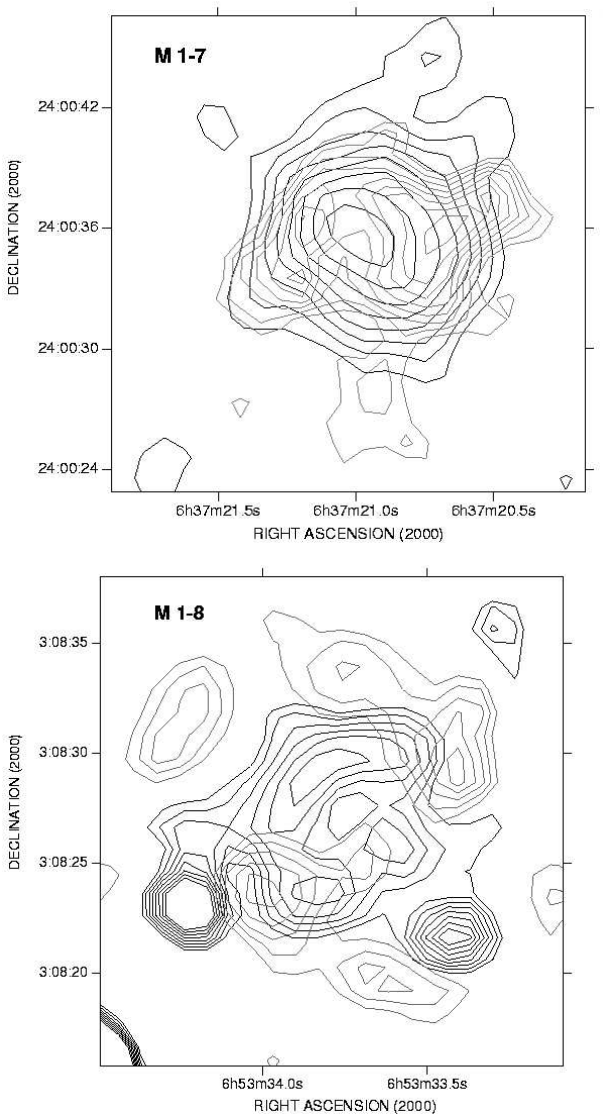

Fig. 7. Maps for M 1−7 and M 1−8, where the H_2 and H band results have been superimposed (H_2 contours are coloured grey).

to whether the observations were affected by the $\lambda 2.11$ μm transition of He I. There are two reasons to believe that this may be the case. Firstly, it would be most unusual to see such strong spatial disconnects between the [N II] and H_2 emission regimes. Similarly, the ring occupies a regime of the shell where He I emission might be expected to be strong.

Taken as a whole, therefore, it is clear that the present procedure for mapping H_2 has produced interesting results, and confirms trends determined from previous narrow band observations. Whilst the method cannot be regarded as a catch-all procedure, and must only be employed under certain stringent conditions, it nevertheless offers an alternative means whereby this emission may be investigated.

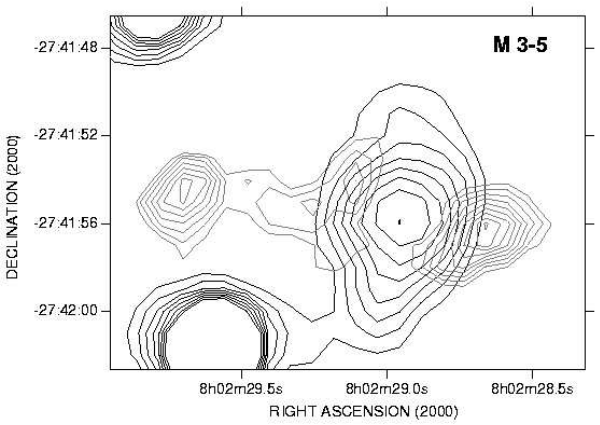

Fig. 8. As in Fig. 7, but for M 3−5. Note the presence of a spatially separated H_2 ansa to the east of the source.

5. CONCLUSIONS

We have used the photometrically accurate, and spatially well-registered 2MASS mapping to determine the distribution of H_2 emission in 14 PNe. The maps of NGC 3132, NGC 6720, and IC 4406 are very similar to those determined in prior narrow band imaging, although they include a broader range of H_2 transitions. They confirm the narrowness of the emission zones, and their apparent extreme fragmentation. Such a tendency is also found in the sources M 1−7, M 1−8, and M 3−5.

Our profiles also confirm the tendency for much of the emission to be located close to, but just outside of the primary ionised zones; a result which is consistent with both of the primary excitation mechanisms. There does appear, however, to be a difference between the sources. More compact (and probably more youthful) outflows show H_2 extensions which are rather large ($\Delta\theta/\theta \sim 0.5 \rightarrow 7$). By contrast, values for the larger (and more evolved) outflows appear significantly smaller (of order $\Delta\theta/\theta \sim 0.03 \rightarrow 0.2$). Although some caution is certainly required, this difference may imply an evolution in the H_2 shells. We have found that if d(H) is the physical size of the nebula as measured in the H band, then $\Delta\theta/\theta \propto \mathrm{d(H)}^{-2.2}$.

The technique presented here may therefore be of great utility in mapping such sources − although its applicability is tightly constrained to certain PNe (those showing no other emission excesses, or localised extinction), and may be applied only where the mapping is accurate and spatially well defined.

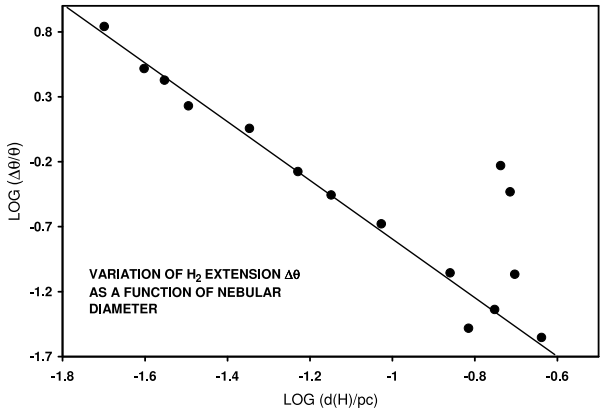

Fig. 9. The logarithmic variation of $\Delta\theta/\theta$ with d(H), the physical size of the outflow. It is clear that $\Delta\theta/\theta$ decreases extremely steeply as the sizes of the envelopes increase.

The only large data base which currently permits such analyses is that created through the 2MASS infrared survey.

This publication makes use of data products from the Two Micron All Sky Survey, which is a joint project of the University of Massachusetts and the Infrared Processing and Analysis Center/California Institute of Technology, funded by the National Aeronautics and Space Administration and the National Science Foundation.

REFERENCES

Aleman, I., & Gruenwald, R. 2004 ApJ, 607, 865
Allen, L. E., Ashley, M. C. B., Ryder, S. D., Storey, J. W. V., Sun, Y.-S., & Burton, M. G. 1997 in IAU Symp. 180, Planetary Nebulae, eds. H. J. Habing, & H. J. G. L. M. Lamers (Dordrecht: Kluwer), 205
Atherton, P. D., Hicks, T. R., Robinson, G. J., Phillips, J. P., Reay, N. K., & Worswick, S. P. 1979, ApJ, 232, 786
Bachiller, R., Forveille, T., Huggins, P. J., & Cox, P. 1997, A&A, 324, 1123
Bachiller, R., Planesas, P., Martin-Pintado, J., Bujarrabal, V., & Tafalla, M. 1989, A&A, 210, 366
Balick, B., Gonzalez, G., Gatley, I., & Zuckerman, B. 1990, in ASP Conf. Ser. Vol. 14, Astrophysics with Infrared Arrays, ed. R. Elston (San Francisco: ASP), 167
Beckwith, S., Persson, S. E., & Gatley, I. 1978, ApJ, 219, L33
Bhatt, H. C., & Mallik, D. C. V. 1986, A&A, 168, 248
Black, J. H., & Dalgarno, A. 1976, ApJ, 203, 132
Black, J. H., & van Dishoeck, E. F. 1987, ApJ, 322, 412
Bohigas, J. 2001, RevMexAA, 37, 237
_____. 2003, RevMexAA, 39, 149
Borkowski, K. J., Harrington, J. P., Blair, W., & Bregman, J. D. 1994, ApJ, 435, 722
Burton, M. G., Hollenbach, D. J., & Tielens, A. G. G. M. 1990, ApJ 365, 620
Cardelli, J. A., Clayton, G. C., & Mathis, J. S. 1989, ApJ, 345, 245
Carpenter, J. M. 2001, AJ, 121, 2851
Cohen, M., & Barlow, M. J. 1974, ApJ, 193, 401
Costero, R., Tapia, M., Mendez, R. H., Echevarría, J., Roth, M., Quintero, A., & Barral, J. F. 1986, RevMexAA, 13, 149
Davis, C. J., Smith, M. D., Stern, L., Kerr, T. H., & Chiar, J. E. 2003, MNRAS, 344, 262
de Marco, O., Crowther, P. A., Barlow, M. J., Clayton, G. F., & de Koter, A. 2001, MNRAS, 328, 527
Deguchi, S., Izumiura, H., Kaifu, N., Mao, X., Nguyen-Q-Rieu, & Ukita, N. 1990, ApJ, 351, 522
Draine, B. T., Roberge, W. G., & Dalgarno, A. 1983, ApJ, 264, 485
Graham, J. R., Herbst, T. M., Matthews, K., Neugebauer, G., Soifer, B. T., Serabyn, E., & Beckwith, S. 1993, ApJ, 408, L105
Greenhouse, M. A., Hayward, T. L., & Thronson, H. A. 1988, ApJ, 325, 604
Guerrero, M. A., Villaver, E., Manchado, A., García-Lario, P., & Prada, F. 2000, ApJS, 127, 125
Hollenbach, D., & McKee, C. F. 1989, ApJ, 342, 306
Hora, J. L., & Latter, W. B. 1994, ApJ, 437, 281
Hora, J. L., Latter, W. B., & Deutsch, L. K. 1999, ApJS, 124, 195
Huggins, P. J., Bachiller, R., Cox, P., & Forveille, T. 1996, A&A, 315, 284
Huggins, P. K., & Healy, A. P. 1989, ApJ, 346, 201
Johnson, H. M., Balick, B., & Thompson, A. R. 1979, ApJ, 233, 919
Josselin, E., & Bachiller, R. 2003, A&A, 397, 659
Kastner, J. H., Gatley, I., Merrill, K. M., Probst, R., & Weintraub, D. A. 1994, ApJ, 421, 600
Kastner, J. H., Weintraub, D.A., Gatley, I., & Henn, L. 2001, ApJ, 546, 279
Kastner, J. H., Weintraub, D. A., Gatley, I., Merrill, K. M., & Probst, R. G. 1996, ApJ, 462, 777
Kwok, S. 2000, The Origin and Evolution of Planetary Nebulae (Cambridge: CUP)
Lame, N. J., Harrington, P., Borkowski, K., & White, S. 1995, BAAS, 27, 1403
Latter, W. B., Kelly, D. M., Hora, J. L., & Deutsch, L. K. 1995, ApJS, 100, 159
Marigo, P., Girardi, L., Groenewegen, M. A. T., & Weiss, A. 2001, A&A, 378, 958
Matsuura, M., Zijlstra, A. A., Molster, F. J., Waters, L. B. F., Nomura, H., Sahai, R., & Hoare, M. G. 2005, MNRAS, 359, 383
Miranda, L. F., Torrelles, J. M., & Eiroa, C. 1995, ApJ, 446, L39

Natta, A., & Hollenbach, D. 1998, A&A, 337, 517
Oloffson, H., Johannson, L., Nguyen-Q-Rieu, Sopka, B., & Zuckerman, B. 1982, BAAS, 14, 895
Peña, M., & Torres-Peimbert, S. 1987, RevMexAA, 14, 534
Phillips, J. P. 2002a, ApJS, 139, 199
_____. 2002b, A&A, 393, 1027
_____. 2003, MNRAS, 344, 501
_____. 2004, MNRAS, 353, 589
_____. 2005, MNRAS, 361, 283
Phillips, J. P., & Ramos-Larios, G. 2005, MNRAS, 364, 849
Phillips, J. P., Sanchez Magro, C., & Martinez Roger, C. 1984, A&A, 133, 395
Pottasch, S. R. 1994, Planetary Nebulae (Dordrecht, Holland: Reidel)
Ramos-Larios, G., & Phillips, J. P. 2005, MNRAS, 357, 732
Rudy, R. J., Lynch, D. K., Mazuk, S., Puetter, R. C., & Dearborn, S. S. P. 2001, AJ, 121, 362
Sahai, R., Hines, D., Kastner, J. H., Weintraub, D. A., Trauger, J. T., Reike, M. J., Thompson, R. I., & Schneider, G. 1998, ApJ, 492, 163L
Schild, H. 1995, A&A, 297, 246
Shupe, D. L., Armus, L., Mattews, K., & Soifer, B. T. 1995, AJ, 109, 1173
Shupe, D. L., Larkin, J. E., Knop, R. A., Armus, L., Matthews, K., & Soifer, B. T. 1998, ApJ, 498, 267
Sternberg, A., & Dalgarno, A. 1989, ApJ, 338, 197
Storey, J. W. V. 1984, MNRAS, 206, 521
Su, K. Y. L., Kelly, D. M., Latter, W. B., Messelt, K. A., et al. 2004, ApJS, 154, 302
Treffers, R. R., Fink, U., Larson, H. P., & Gautier, T. N. 1976, 209, 793
Vicini, B., Natta, A., Marconi, A., Testi, L., Hollenbach, D., & Draine, B. T. 1999, A&A, 342, 823
Whitelock, P. A. 1985, MNRAS, 213, 59
Willner, S. P., Becklin, E. E., & Visvanathan, N. 1972, ApJ, 175, 699
Willner, S. P., Jones, B., Puetter, R. C., Russell, R. W., & Soifer, B. T. 1979, ApJ, 234, 496
Zhang, C. Y. 1995, ApJS, 98, 659
Zhang, C. Y., & Kwok, S. 1992, ApJ, 385, 255
Zuckerman, B., & Gatley, I. 1988, ApJ, 324, 501

Simon N. Kemp, John P. Phillips, and Gerardo Ramos-Larios: Instituto de Astronomía y Meteorología, Universidad de Guadalajara, Av. Vallarta No. 2602, Col. Arcos Vallarta, 44130 Guadalajara, Jalisco, México (gerardo@astro.iam.udg.mx, jpp@cencar.udg.mx, snk@astro.iam.udg.mx).